The Role of sp^3 Defects in Eliciting Divergent Fluorescence Response of Single-Walled Carbon Nanotubes to Dopamine and Serotonin

Srestha Basu,[a] Adi Hendler-Neumark,[a] and Gili Bisker[*a,b,c,d]

[a] Department of Biomedical Engineering, Faculty of Engineering, Tel Aviv University, Tel Aviv 6997801, Israel

[b] Center for Physics and Chemistry of Living Systems, Tel Aviv University, Tel Aviv 6997801, Israel

[c] Center for Nanoscience and Nanotechnology, Tel Aviv University, Tel Aviv 6997801, Israel

[d] Center for Light-Matter Interaction, Tel Aviv University, Tel Aviv 6997801, Israel

Email: bisker@tauex.tau.ac.il

Keywords: single-walled carbon nanotubes, defects, neurotransmitters, fluorescence, dopamine, serotonin

Abstract:

Modulating the optical response of fluorescent nanoparticles through rational modification of their surface chemistry can yield distinct optical signatures upon the interaction with compositionally analogous molecules. Herein, we present a novel method for tuning the fluorescence response of single-walled carbon nanotubes (SWCNTs) towards dopamine (DA) and serotonin, two compositionally similar monoamine-hydroxylated aromatic neurotransmitters, by introducing oxygen defects into (6,5) chirality-enriched SWCNTs suspended by sodium cholate (SC). This modification facilitated opposite optical responses towards these neurotransmitters, where DA significantly increased the fluorescence of the defect-induced SWCNTs (D-SWCNTs) six-fold, while serotonin notably decreased it. In contrast, pristine, defect-free SWCNTs exhibited similar optical responses to both neurotransmitters. The underlying mechanisms for the divergent fluorescence response were found to be polydopamine (PDA) surface adsorption in the case of DA's fluorescence enhancement, while serotonin's fluorescence decrease was attributed to enhanced solvent relaxation effects in the presence of defects. Importantly, the divergent optical response between DA and serotonin by D-SWCNTs via the introduction of defects was validated in complex biological environments, such as serum. Further, the generality of our approach was confirmed by the successful demonstrations of a divergent fluorescence response of D-SWCNT suspended by an additional dispersant, namely lipid–polyethylene glycol (PEG). This study offers promising avenues for the broad applicability of tailored surface functionalization of SWCNTs to achieve divergent responses towards compositionally similar molecules and advance innovative applications in sensing, imaging, and diagnostic technologies.

1. Introduction:

The interaction of optical probes with exogenously added molecules is primarily dictated by the chemical composition of these molecules, resulting in alterations in the optical signatures of the probes, thereby enabling the successful detection of the target molecules.[1, 2] Therefore, molecules with similar compositional features often elicit similar optical responses from the probes, making their clear-cut distinction a significant challenge.[3, 4] Thus, the development of techniques for tailored functionalization of optical probes that give rise to divergent optical responses toward compositionally analogous analytes is a challenge worthy of pursuit.

To this end, single-walled carbon nanotubes (SWCNTs), which exhibit fluorescence in the beneficial near-infrared (NIR) region and feature noteworthy photostability, ease of surface functionalization, biocompatibility, tunable surface chemistry, and fluorescence modulation following analyte binding and surface composition, have emerged as optical probes capable of responding to a wide array of analytes.[5-9] These include proteins,[10-12] lipids,[13] sugars,[14-16] hormones, metal ions,[17] oncometabolites,[18] volatiles,[19, 20] pathogens,[21, 22] micro-RNA,[23, 24] neurotransmitters,[25-29] enzyme activity, and inhibition,[30-32] among others. Furthermore, SWCNTs are known for their well-defined graphene-like surfaces, which largely govern their interactions with exogenously added molecules. Thus, tailoring the surface of SWCNTs with functional modalities presents an interesting and realistic approach to tuning their surface chemistry. This, in turn, enables the customization of their responses to molecule libraries sharing common features that would otherwise evoke similar optical responses of the SWCNTs.

In this context, a promising technique for introducing tailored functionalities into SWCNTs involves the incorporation of sp^3 defects.[33-44] These deliberately introduced defects not only lead to the emergence of intriguing optical properties but also provide an additional platform for selective interaction with chosen analytes, thereby paving the way for selective molecular recognition. In this regard, aryl defects-incorporated SWNCTs have been used as sensors for the detection of a number of analytes.[45-48] However, the utility of exogenously incorporated defects in SWCNTs for modulating their optical response toward a particular analyte is largely unprecedented in the literature. Furthermore, achieving starkly divergent optical responses to two compositionally analogous molecules, thereby paving the way for their successful discrimination, could be a direct consequence of the surface functionalization of SWCNTs with defects. This approach not only holds significant promise for advancing the field of selective molecular recognition using SWCNTs but also lays the groundwork for deterministic modulation of the surface chemistry of SWCNTs to achieve tailored optical responses.

Among a wide variety of compositionally similar molecules, neurotransmitters stand out as particularly important due to their similar functional groups and parallel compositional frameworks.[49, 50] Despite these compositional similarities, each neurotransmitter exerts distinct effects on the neurological system. For instance, DA and serotonin are both monoamine-based neurotransmitters that share hydroxyl groups and aromatic rings. However, their impacts on the neurological system differ

significantly. Given their compositional similarities, it would be straightforward to expect similar optical responses to any optical probe, such as NIR fluorescent SWCNTs. However, their starkly divergent impacts on health, behavior, and diseases emphasize the importance of developing techniques that use the principles of chemistry to tune the surface functionalization of SWCNTs. This tuning would enable the SWCNTs to react and generate contrasting optical responses to compositionally similar neurotransmitters like DA and serotonin. Achieving such divergent effects from compositionally close molecules, by virtue of the introduction of oxygen defects in SWCNTs, holds great potential not only for advancing our understanding of the chemical behavior of these neurotransmitters, which play vital roles in neurological function and disorders but also for the development of tools to allow tailored optical responses from optical probes.

Herein, we report an approach of introducing substitutional defects in SWCNTs to achieve distinctive fluorescence responses when exposed to DA and serotonin (Scheme 1), which otherwise evoked allied optical responses from SWCNTs without defects. To this end, oxygen defects were introduced into sodium cholate (SC) suspended SWCNTs via reaction with sodium hypochlorite under UV irradiation. UV-vis-NIR absorbance, NIR fluorescence, and Raman spectroscopic studies verified the successful incorporation of the oxygen defects in the SC-SWCNTs. Remarkably, DA and serotonin, despite sharing the characteristic of being monoamine-hydroxylated aromatic neurotransmitters, demonstrated divergent effects on the fluorescence of the D-SWCNTs. Specifically, DA caused a notable six-fold increase in the fluorescence intensity of the D-SWCNTs, while serotonin resulted in a significant intensity decrease. Notably, the distinction between DA and serotonin was minimal when pristine SWCNTs without defects were employed. The amount of defects introduced into the SWCNTs, characterized by the E_{11} to E_{11}^* peak ratio, played a critical role in distinguishing DA and serotonin. Explorations into the mechanisms through Raman spectroscopy and electrospray ionization mass spectrometry unveiled that the remarkable enhancement in the fluorescence intensity of D-SWCNTs when exposed to DA could be attributed to the surface adsorption of D-SWCNTs by polydopamine (PDA). In contrast, the significant decrease in the fluorescence intensity of D-SWCNTs upon exposure to serotonin could be attributed to enhanced solvent relaxation of the SWCNTs in the presence of oxygen defects. Moreover, the effectiveness of defects in generating contrasting optical responses SWCNTs to DA and serotonin has been demonstrated in complex biological environments, such as fetal bovine serum (FBS). Furthermore, the generality of the principle of using sp^3 defects to modulate the optical responses of SWCNTs towards DA and serotonin has been validated with defect-induces SWCNTs suspended by Polyethylene glycol (PEG)-lipid corona. Our findings not only mark the first instance of DA and serotonin optical differentiation using defect-incorporated SWCNTs but also offer promising avenues for tailored surface functionalization of SWCNTs for advancing their innovative applications in sensing, imaging, and diagnostic technologies.
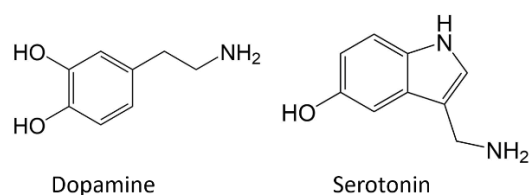
**Scheme 1:** Molecular structures of DA and serotonin

2. Results and discussions:

2.1. Incorporation of oxygen defects into sodium cholate (SC) SWCNTs:

The introduction of oxygen defects into (6,5) enriched SC-SWCNTs was accomplished through a minor modification of a previously established procedure[51] involving the reaction of controlled amounts of SC-SWCNTs and NaClO under UV irradiation. To assess the impact of oxygen defects, the UV-vis-NIR absorption spectrum of pristine SC-SWCNTs was compared to that of the D-SWCNTs (**Figure 1 a**). In agreement with prior findings,[51] the absorption peak associated with the E_{11} transitions in pristine SC-SWCNTs at 988 nm slightly decreased after incorporating oxygen defects as a result of the perturbations induced by the covalent modifications. It is important to note that the chemical bonding of oxygen defects within SWCNTs is reported to occur through the formation of ether or epoxide.[51-53]

Subsequently, Raman spectra of both pristine SC-SWCNTs and D-SWCNTs were obtained to confirm the successful inclusion of oxygen defects. Consistent with previous literature reports, the introduction of point-like defects in the otherwise sp^2 carbon lattice increased the Raman D mode, in addition to the existing G band. Accordingly, the Raman spectra of D-SWCNTs displayed the emergence of a D band at 1312 cm^{-1}, alongside the G band at 1587 cm^{-1}, validating the incorporation of oxygen defects into SC-SWCNTs (**Figure 1 b**).[47, 54]

The time-dependent fluorescence spectra of SC-SWCNTs incubated with NaClO under UV irradiation were also monitored to assess the effect of the defects on the SWCNT fluorescence. The successful incorporation of oxygen defects was evidenced by the gradual appearance of a fluorescence peak at 1120 nm (E_{11}^*), in addition to the existing peak at 988 nm (E_{11}). As evinced from the normalized fluorescence spectra of SC-SWCNTs before and after treatment with NaClO, with an increase in UV exposure from 1-4 min, the peak at 1120 nm exhibited a gradual augmentation (**Figure 1 c**). Notably, the overall fluorescence of the SC-SWCNTs decreased following the incorporation of defects (**Figure S1**). This observation suggests the potential depopulation of higher energy bright E_{11} states, thereby leading to the overall decrease in the fluorescence of the SWCNTs.[55-57] In conjunction, the corresponding excitation-emission profile of the D-SWCNT fluorescence was recorded as a function of increasing defect concentration. These profiles featured the progressive emergence of the fluorescence peak attributed to E_{11}^*, thus clearly confirming the successful introduction of oxygen defects (**Figure 1 d-g**). An important observation from these results was that the number of defects in the D-SWCNTs could be regulated by controlling the duration of UV irradiation.
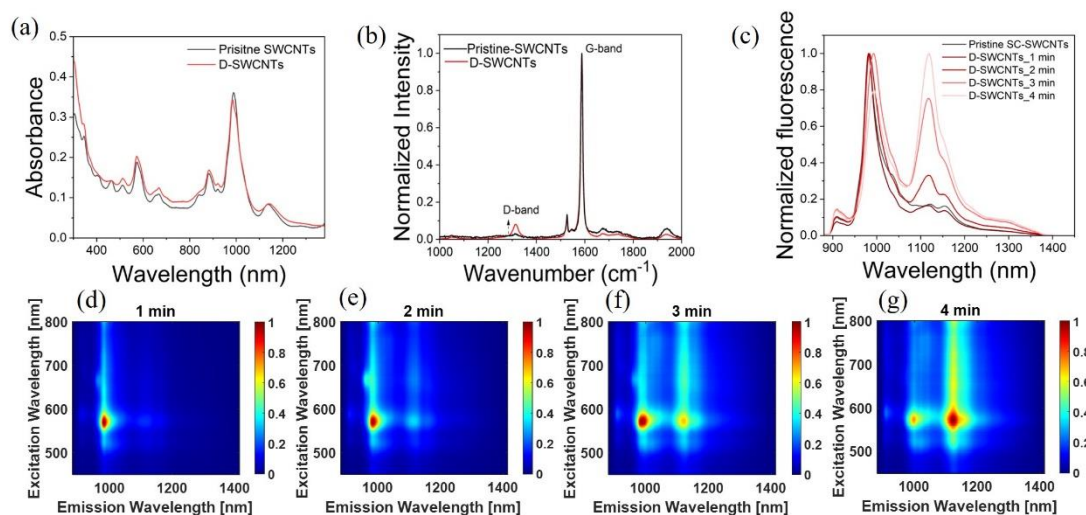
Figure 1. (a) UV-vis-NIR absorption spectra of pristine SC-SWCNTs (black curve) and D-SWCNTs (red curve). **(b)** Raman spectra of pristine SC-SWCNTs (black curve) and D-SWCNTs (red curve). **(c)** Normalized fluorescence spectra of SC-SWCNTs upon addition of NaClO with increasing duration of UV irradiation. Excitation-emission map of D-SWCNTs with UV exposure for **(d)** 1 min, **(e)** 2 min, **(f)** 3 min, and **(g)** 4 min.

2.2 Modulating the response of DA and serotonin towards SWCNTs by the introduction of sp^3 defects:

Having confirmed the successful incorporation of oxygen defects in chirality-enriched SC-SWCNTs, we then focused on evaluating their efficacy as probes for modulating the optical response of compositionally related analytes with similar functional groups. Neurotransmitters, which typically consist of allied functional groups and thus result in similar optical responses of conventional probes, were chosen as model analytes. Our objective was to determine if the introduction of sp^3 defects in SWCNTs could differentiate these analytes by altering their optical interactions with the SWCNTs.

Control experiments were first conducted using pristine (6,5) enriched SC-SWCNTs, devoid of defects, incubated with DA and serotonin. Interestingly, the fluorescence intensity of pristine SC-SWCNTs exhibited a decrease of approximately 10% upon the addition of DA. Moreover, the fluorescence of SC-SWCNTs was quenched by about 28%, accompanied by a red shift of 4 nm upon adding serotonin (**Figure 2 a**). Thus, it was clear that pristine SC-SWCNTs, in the absence of defects, evoked rather similar optical responses of the SWCNTs. On a similar note, instead of (6,5) enriched SC-SWCNTs, SWCNTs with mixed chirality dispersed with SC were incubated with DA and serotonin, and the resultant fluorescence spectra were recorded (**Figure S2**). Interestingly, DA did not lead to any discernible change in the fluorescence of the SC-SWCNTs, while serotonin led to a ~18% decrease in the fluorescence intensity. The immediate next challenge was to determine if (6,5) enriched SWCNTs, which were similarly responsive to DA and serotonin, could exhibit differentiated optical responses upon the incorporation of defects.

Thus, in the next step, D-SWCNTs were incubated with DA and serotonin. In this set of experiments, the degree of defects in D-SWCNTs was controlled to a point where

the fluorescence peak height associated with E_{11}^* surpassed that of E_{11}. Intriguingly, upon the introduction of oxygen defects, DA increased the fluorescence intensity of D-SWCNTs by a factor of ~6. On the contrary, serotonin led to a significant decrease by a factor of ~0.8 in the fluorescence intensity (**Figure 2 b**). The diverse fluorescence responses of D-SWCNTs to compositionally analogous neurotransmitters not only highlight the role of surface functionalities in nanoscale particles as a tool to alter their interactions with similar analytes but also pave the way for establishing them as effective probes for discriminating between these analytes.

In addition to the D-SWCNT sample in which the E_{11}^* peak was greater than E_{11} (**Figure 2 b**), we prepared two additional dispersions of D-SWCNTs with distinct levels of defects characterized by different E_{11} to E_{11}^* ratios, having E_{11} nearly equal to E_{11}^* (**Figure 2 c**), and E_{11} greater than E_{11}^* (**Figure 2 d**), to test the effect of defect density. Upon exposure to DA, the increase in D-SWCNTs$_{E11>E11*}$ fluorescence intensity was less than that of D-SWCNTs$_{E11<E11*}$. On the other hand, the fluorescence intensity of both D-SWCNTs$_{E11>E11*}$ and D-SWCNTs$_{E11<E11*}$ was significantly decreased upon interaction with serotonin. The largest fluorescence increase was observed in the case of D-SWCNTs$_{E11\sim\,=E11*}$. Nevertheless, the fluorescence of D-SWCNTs$_{E11\,=\,E11*}$ was nearly non-responsive to serotonin.
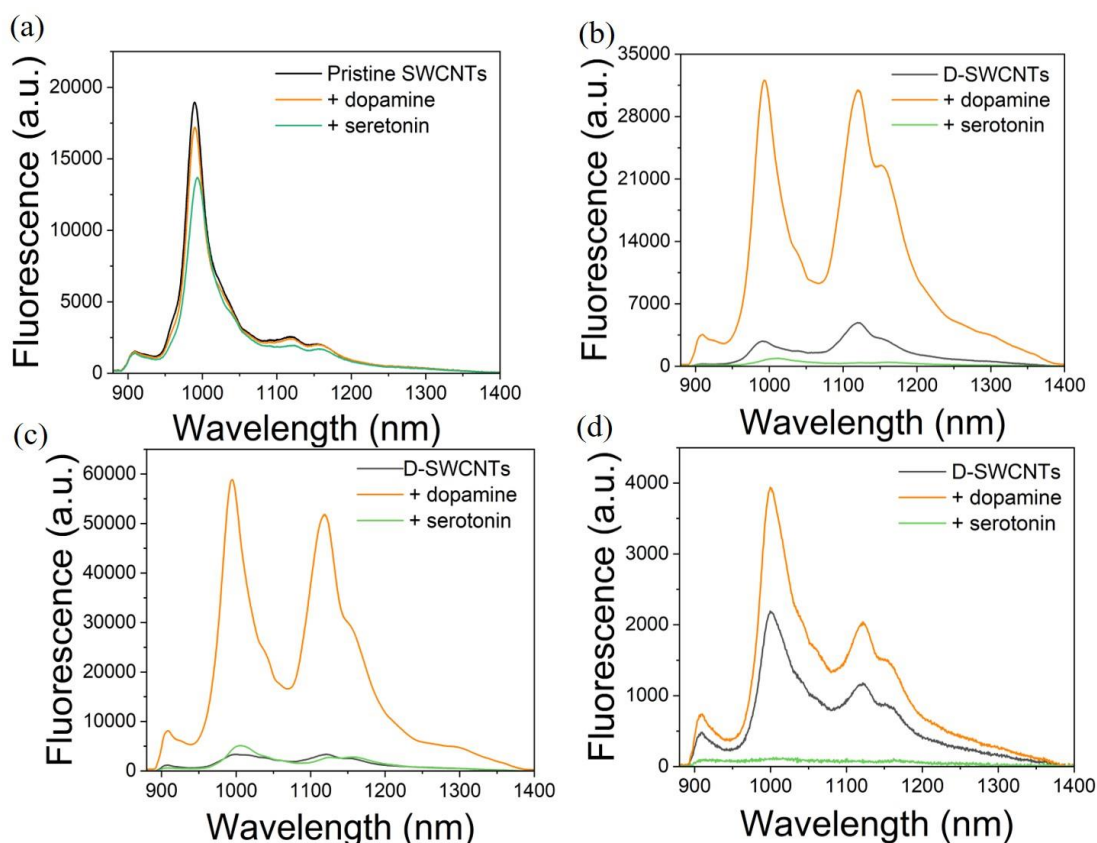
Figure 2. (a) Fluorescence spectra of pristine SC-SWCNTs (black curve) and that following the addition of dopamine (orange curve) and serotonin (green curve). **(b)** Fluorescence spectra of D-SWCNTs before (black curve) and after the addition of DA (orange curve) or serotonin (green curve), for D-SWCNTs with $E_{11} > E_{11}^*$, **(c)** $E_{11} = E_{11}^*$, and **(d)** $E_{11} < E_{11}^*$.

These results underscore the pivotal role of defect density within SWCNTs in eliciting divergent responses from DA and serotonin. Based on these findings, it can be inferred that, for optimal discrimination of DA and serotonin, D-SWCNTs with $E_{11} < E_{11}^*$ would be an optimal choice. Therefore, D-SWCNTs$_{E_{11}<E_{11}^*}$ was selected for further experimentation, as detailed in the subsequent sections.

Additionally, the UV-vis-NIR absorption spectra of D-SWCNTs were recorded before and after the introduction of DA and serotonin (**Figure S3**). The peak at 988 nm in D-SWCNTs, associated with E_{11} transitions, demonstrated a decrease of approximately 7% upon adding DA. On the other hand, adding serotonin to D-SWCNTs resulted in a decrease of about 12% in the absorbance of the peak at 988 nm, accompanied by a bathochromic shift of approximately 10 nm. These findings, in line with previous studies, emphasize that the changes in the fluorescence of D-SWCNTs upon adding DA and serotonin could be attributed to physicochemical interactions between D-SWCNTs and the respective analytes.[58]

2.3. Effect of monoamine compounds on the fluorescence of D-SWCNTs:

Among the various commonalities in the compositional features of DA and serotonin, the presence of a single amine group is particularly notable. To further understand the role of amine groups in modulating the fluorescence of D-SWCNTs to DA and serotonin vis-à-vis pristine SWCNTs, D-SWCNTs with $E_{11}^* > E_{11}$ were incubated with several other neurotransmitters, including histamine, glutamic acid, γ-aminobutyric acid (GABA), and glycine, alongside DA and serotonin. The rationale for choosing these neurotransmitters as model examples was based on their composition, having a single amine group. Additionally, some of these neurotransmitters have aliphatic chains, while others, such as histamine, contain aromatic rings (namely imidazole). The corresponding fluorescence spectra were recorded (**Figure S4**). Interestingly, glycine, GABA, and glutamic acid – the three aliphatic amines – caused an increase in the fluorescence intensity of D-SWCNTs by a factor of ~1-2, while histamine, composed of an aromatic ring, led to an intensity increase by a factor of ~3. It was interesting to observe that aromatic ring-containing neurotransmitters were found to elicit a greater increase in the fluorescence of D-SWNCTs as opposed to aliphatic chain-containing neurotransmitters. However, neurotransmitters with (mono) amine groups, regardless of the presence or absence of aromatic rings, were found to augment the fluorescence of D-SWCNTs. Notably, the increase in the fluorescence of D-SWCNTs upon interaction with these neurotransmitters was significantly lower compared to DA, which enhanced the fluorescence of D-SWCNTs by a factor of approximately 6, despite having common compositional features like amine groups, aromatic rings, and hydroxyl groups.

Additionally, we investigated the effect of other monoamine-based molecules, not categorized as neurotransmitters, on the fluorescence response of D-SWCNTs. To this end, levodopa (L-DOPA), ortho-aminophenol (OAP), L-tryptophan, and L-serine were incubated with D-SWCNTs, and the corresponding fluorescence spectra were recorded (**Figure S5**). Intriguingly, these monoamine-based molecules were observed to exert a slight (~15%) enhancement in the fluorescence intensity of D-SWCNTs, particularly in the E_{11}^* peak at 1120 nm, which is attributed to the defects. This result further highlights

that while amine-containing molecules can increase the fluorescence of defect-incorporated SWCNTs, the most prominent increase is caused by DA. In contrast, serotonin, which also contains a monoamine group, was found to significantly decrease the fluorescence of the D-SWCNTs.

2.4. Calibration of D-SWCNTs for DA and serotonin:

Having confirmed that the introduction of oxygen defects in SC-SWCNTs results in divergent effects of DA and serotonin on the fluorescence of the D-SWCNTs, an outcome not achievable without defect incorporation, we aimed to investigate the change in the fluorescence of D-SWCNTs upon the addition of varying concentrations of DA and serotonin. In this pursuit, the fluorescence intensities of the peaks at 988 nm and 1120 nm, attributed to E_{11} and E_{11}^* transitions, respectively, were observed to increase upon the addition of increasing concentrations of DA (**Figure 3 a**). The normalized fluorescence responses of both E_{11} and E_{11}^* peaks were fitted using a Hill equation (**Figure 3 b, Table S1**). The obtained dissociation constant K_d values from the fitting of E_{11} and E_{11}^* were determined to be 73.6 ± 8.8 μM and 51 ± 9.5 μM, respectively. The limit of detection (LOD) for DA by D-SWCNTs was calculated to be 3.7 ± 0.68 μM.

On the other hand, upon adding varying concentrations of serotonin to D-SWCNTs, the fluorescence intensities of the peaks at 988 nm and 1120 nm decreased (**Figure 3 c**). In this case, the fluorescence response of the E_{11} and E_{11}^* peaks could also be fitted with a Hill equation (**Figure 3 d**, Table S1). The K_d values calculated from the fitting of E_{11} and E_{11}^* peaks were found to be 2.6 ± 0.6 μM and 2.8 ± 0.5 μM, respectively. The LOD of serotonin was calculated to be 0.25 ± 0.027 μM. The obtained LODs for DA and serotonin by D-SWCNTs are comparable to those obtained by other techniques, including colorimetry,[59] conductivity,[60] cyclic voltammetry,[61] and visible range fluorometry.[62]
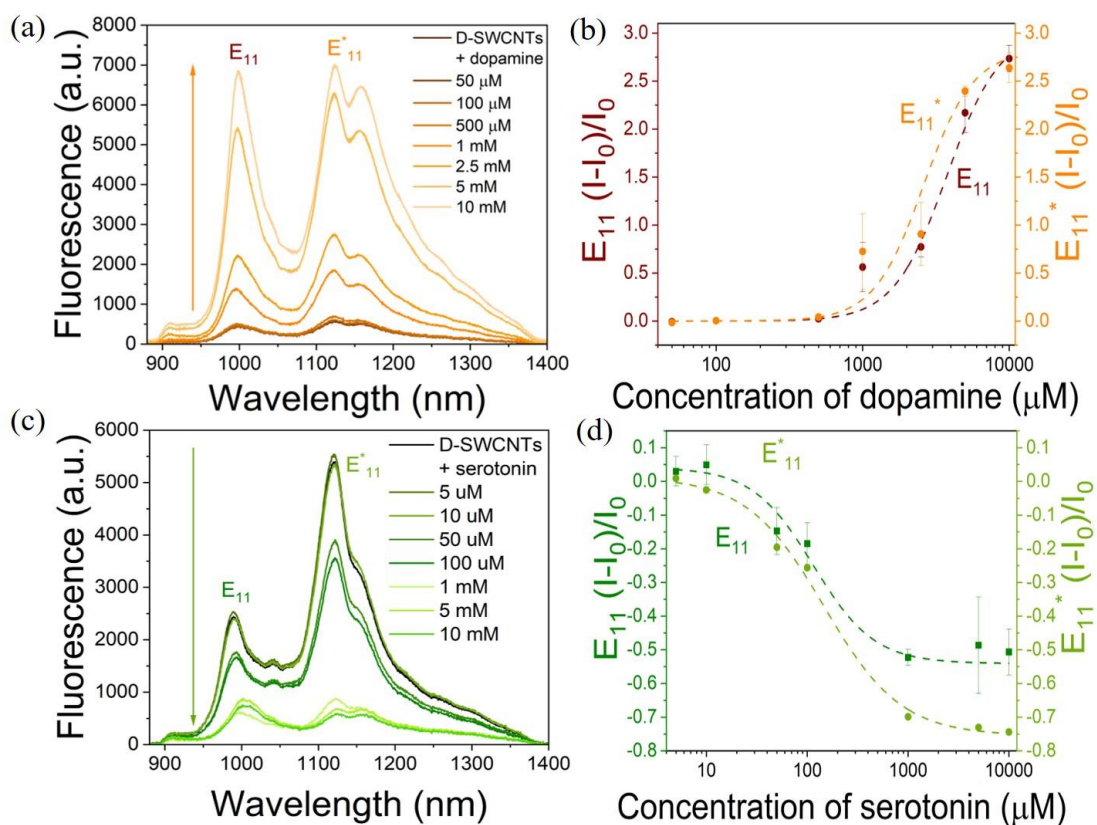
Figure 3. **(a)** Fluorescence spectra of D-SWCNTs before and after the addition of varying concentrations of DA. **(b)** Normalized fluorescence response of E_{11} (orange) and E_{11}^* (brown) peaks of D-SWCNTs towards varying concentrations of DA. **(c)** Fluorescence spectra of D-SWCNTs before and after the addition of varying concentrations of serotonin. **(d)** Normalized fluorescence response of E_{11} (dark green) and E_{11}^* (light green) peaks of D-SWCNTs towards varying concentrations of serotonin.

2.5. *Underlying mechanism governing the fluorescence intensity enhancement of D-SWCNTs by DA:*

Having established the concentration-dependent divergent effects of DA and serotonin on the fluorescence of D-SWCNTs while also confirming the indispensable role of defects in achieving these effects, we aimed to understand the mechanism underlying the enhancement in the fluorescence intensity of D-SWCNTs upon adding DA.

The enhancement in the fluorescence intensity of pristine SWCNTs without defects upon interaction with DA is commonly attributed to the removal of reactive oxygen species (ROS).[63] DA, being a redox-active molecule, can scavenge oxygen radicals. Additionally, it is well-established that the fluorescence of SWCNTs can be effectively quenched in the presence of ROS.[63] Therefore, the removal of ROS due to their scavenging by DA is likely to increase the fluorescence intensity of the SWCNTs. However, in our study, the ROS of concern is singlet oxygen species, which have limited lifetimes in water, on the order of microseconds, suggesting that the effect of ROS would be minimal.[64] Nevertheless, to investigate if the ROS-based mechanism of

fluorescence enhancement applies to defect-induced SWCNTs as well, we tested this possibility with D-SWCNTs. For this, we incubated pristine and D-SWCNTs with mannitol, a well-known radical scavenger. However, while the fluorescence of pristine SWCNTs remained practically unaltered, the fluorescence of D-SWCNTs showed a slight increase following interaction with mannitol, suggesting that the scavenging of oxygen radicals could not fully explain the enhancement in the fluorescence intensity of D-SWCNTs by DA (**Figure S6**).

Another plausible mechanism frequently invoked to elucidate the phenomenon of fluorescence enhancement in various nanoscale particles is that of surface passivation.[65-68] Surface passivation is known to enhance the fluorescence of nanoparticles by reducing non-radiative decay, a process that competes with radiative channels, thereby increasing the fluorescence quantum yield.[67] Passivating molecules on the surface can limit the access of molecules that cause fluorescence quenching, preventing solvent relaxation and spatial proximity of other quenchers. Additionally, surface defects may induce non-radiative states, and passivation can mitigate these effects, resulting in a substantial enhancement in the fluorescence of nanoparticles.[69] We postulated that surface passivation might be a conceivable mechanism for the fluorescence enhancement of D-SWCNTs induced by DA. This speculation is based on the known propensity of DA to readily generate PDA, especially in an oxidative environment, which could potentially passivate the surface of D-SWCNTs, resulting in an augmented fluorescence signal.[70] However, in our case, owing to the potential ability of the formed PDA to physically adsorb onto the surface of SWCNTs, we use the term 'adsorption' in our subsequent discussion.

To further validate the potential formation of PDA from DA in the presence of D-SWCNTs, we initially examined the feasibility of PDA generation. The confirmation of PDA formation was obtained through electrospray ionization mass spectrometry (ESI-MS) analysis (**Figure S7 a**), revealing a major peak at 227 Da,[71] corresponding to the mass of a fragment of PDA. Further, additional peaks were observed due to the fragmentation of PDA, which have been assigned to specific chemical formulas in Table S2. In contrast, the ESI-MS spectrum of DA-added pristine SWCNTs showed major peaks at 154 Da (DA monomer) and 431 Da (sodium cholate), with no signature peak of PDA observed (**Figure S7 b**). This also highlights the essential role of oxygen defects in mediating the transformation of DA to PDA and subsequent enhancement of D-SWCNT fluorescence upon DA addition, an effect not observed in SWCNTs lacking oxygen defects. To further substantiate the attribution of the 227 Da peak to PDA fragmentation, ESI-MS spectra of pristine and D-SWCNTs without the addition of DA were also acquired (**Figure S7 c-d**). Interestingly, no discernible peak at 227 Da was observed in these spectra, affirming that the peak associated with PDA originated solely from monomeric DA.

Having established the formation of PDA, our subsequent objective was to further substantiate the role of oxygen defects in the conversion of DA to PDA. It is worth-mentioning here that the essential role of oxygen defects in converting DA to PDA, and thereby causing an enhancement in the fluorescence of D-SWCNTs, seemed rather intuitive. This intuition was supported by existing literature, which reports that the introduction of aryl defects into SWCNTs, which do not promote the conversion of

DA to PDA, results in a decrease in fluorescence upon the addition of DA.[45] This suggests that oxygen defects could be crucial for the observed fluorescence enhancement in the presence of DA, as they likely facilitate the transformation of DA to PDA in an oxidative environment. To address this, we utilized Raman spectroscopy to scrutinize potential changes in the D band associated with defects upon adding DA. The Raman spectra of D-SWCNTs were recorded before and after the introduction of DA (**Figure 4**). Intriguingly, the intensity of the D band decreased upon the addition of DA, providing clear evidence of a chemical interaction between the defects within D-SWCNTs and DA. Furthermore, upon the addition of DA to D-SWCNTs, a peak at 1089 cm^{-1} emerged, typically originating from pentagonal defects in SWCNTs.[72] Thus, in our case, it might be possible that the PDA molecules formed due to oxygen defects mediated conversion of DA might have been adsorbed onto the surface of SWCNTs, leading to some distortion in the hexagonal units. This distortion might have resulted in the conversion of some hexagonal units to pentagonal units, as indicated by the emergence of the peak at 1089 cm^{-1}. These additional evidences support the ubiquitous role of oxygen defects in the transformation of DA to PDA and the subsequent adsorption of PDA onto the surface of SWNCTs, ultimately leading to an enhancement in the fluorescence intensity of D-SWCNTs. Further, the validity of our claim regarding the adsorption of PDA onto the surface of D-SWCNTs leading to surface adsorption was further supported by normalizing the fluorescence spectra of D-SWCNTs before and after the addition of dopamine. After normalizing the spectra to the E_{11} peak, we observed a decrease in the intensity of the E_{11}* peak (**Figure S8**). This indicates that while the addition of dopamine results in an overall increase in the fluorescence of D-SWCNTs, the relative contribution of the defects to the emitted fluorescence has decreased following the adsorption of PDA.
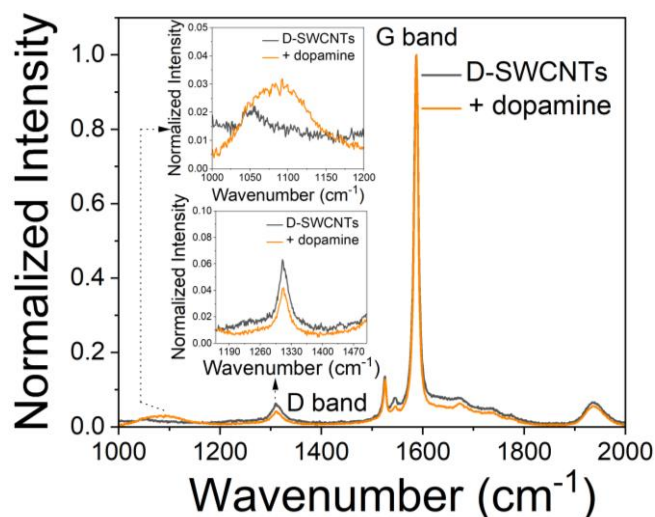
Figure 4. Raman spectra of D-SWCNTs before (black) and after the addition of DA (orange).

A schematic illustrating the plausible surface adsorption of D-SWCNTs by DA and the subsequent enhancement in the fluorescence of D-SWCNTs is shown in **Scheme 2**.
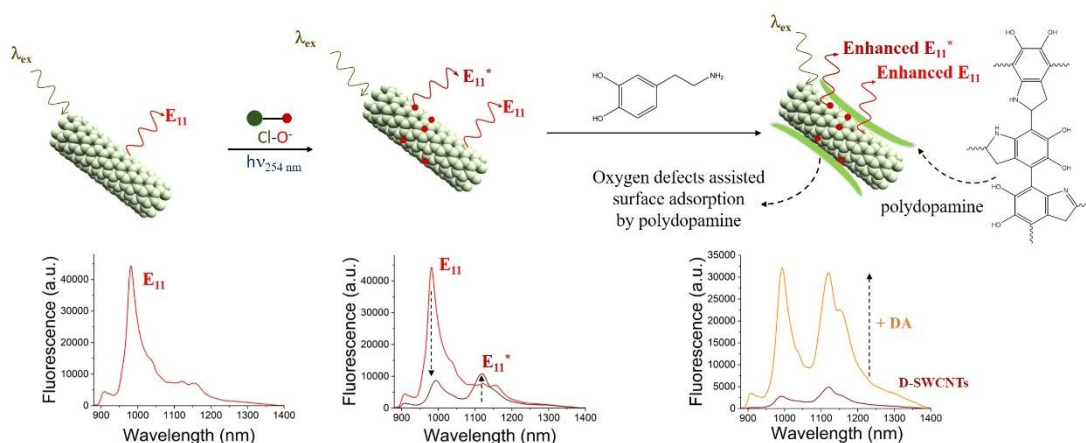
Scheme 2. Schematic illustration of oxygen-defect introduction into SWCNT by exposure to NaClO under UV light (254 nm), resulting in the appearance of a new peak at 1120 nm, attributed to E_{11}^{*} transitions and an overall decrease in the fluorescence intensity of D-SWCNTs compared to pristine SWCNTs. Subsequently, the introduction of DA results in increased fluorescence intensity of the D-SWCNTs through the proposed mechanism of surface adsorption by PDA.

2.6. Underlying mechanism governing the fluorescence intensity decrease of D-SWCNTs by serotonin:

In the subsequent phase, we aimed to unravel the plausible mechanism through which the fluorescence of D-SWCNTs was quenched upon the addition of serotonin. One potential scenario could involve a direct interaction between the defects present within the SWCNTs and serotonin, resulting in fluorescence modulation. However, Raman spectra of D-SWCNTs before and after adding serotonin showed no noticeable change in the D band of D-SWCNTs, associated with defects, upon the addition of serotonin (**Figure S 9**). This suggests that the fluorescence quenching of D-SWCNTs by serotonin did not result from a direct chemical interaction between the defects and serotonin.

On a different note, a noteworthy observation was that in the absence of defects, serotonin quenched the fluorescence of pristine SC-SWCNTs by approximately 28% (**Figure 2 a**). Interestingly, this extent of fluorescence reduction in SWCNTs by serotonin became more pronounced upon introducing defects, indicating that the defects further amplified the effect already present before their introduction. As discussed previously, the decrease in the fluorescence of pristine SC-SWCNTs upon adding serotonin was generally attributed to enhanced water accessibility due to changes in the surface coverage of SWCNTs.[73] In this context, the increase in water accessibility is likely to be more pronounced in the presence of oxygen defects, potentially facilitated by hydrogen bonding between water molecules and oxygen defects within the SWCNTs. Consequently, the magnitude of the normalized fluorescence intensity decrease in D-SWCNTs upon adding serotonin might be more pronounced compared to pristine SWCNTs due to enhanced water accessibility facilitated by hydrogen bonding with the oxygen defects. This was further validated by the normalized spectra of D-SWCNTs before and after the addition of serotonin, where

normalizing the spectra to the E_{11} peak revealed an independent decrease in the intensity of the defect-related peak (**Figure S10**).

In this regard, electronic-to-vibrational energy transfer (EVET) to H_2O molecules may also contribute to the observed decrease in fluorescence of D-SWNCTs upon the addition of serotonin.[45] To investigate this, we examined the effect of adding serotonin to D-SWCNTs in a D_2O environment. This experiment was based on the fact that H_2O absorbs in the NIR region, whereas D_2O does not. Therefore, if EVET played a role in decreasing the fluorescence of D-SWCNTs upon the addition of serotonin in H_2O, the addition of serotonin in D_2O would be expected to significantly reduce the extent of the fluorescence response. Specifically, we introduced defects in the SWCNTs in a D_2O environment, dissolved serotonin in D_2O, and then added the serotonin to the D-SWCNTs. In an H_2O environment, which absorbs in the NIR window, the addition of serotonin resulted in an approximately 85% decrease in the fluorescence of D-SWCNTs. However, in a D_2O environment, the decrease was only around 20% (**Figure S11**). This significant difference in the response of D-SWCNTs to serotonin in H_2O and D_2O environments clearly highlights the critical role of H_2O in EVET from D-SWCNTs. Thus, we attribute the decreased fluorescence of D-SWCNTs upon the addition of serotonin to EVET, further substantiating our proposed mechanism.

On the other hand, in line with PDA formation, as observed in the earlier section, we wanted to check the possibility of polyserotonin formation owing to the presence of oxygen defects in SWCNTs. To investigate the possibility of polyserotonin formation contributing to the decrease in fluorescence of D-SWCNTs following the addition of serotonin, we recorded the ESI-MS spectra of pristine and D-SWCNTs after serotonin addition (**Figure S12 a-b**). However, neither spectrum exhibited peaks corresponding to fragments of polyserotonin. As evinced from **Figure S12 a-b**, the peaks observed at 160 Da, 175 Da, and 431 could be ascribed to the fragmentation of serotonin (following the release of ammonia), parent serotonin, and SC, respectively. This negated the possibility of a contribution of polyserotonin to the observed decrease in the fluorescence of D-SWCNTs.

2.7. Divergent response of D-SWCNTs to DA and serotonin in blood serum:

To validate the role of sp^3 defects in the successful modulation of fluorescence response of SWCNTs DA and serotonin in real-world samples, we evaluated their performance in fetal bovine serum (FBS). Initially, we introduced varying concentrations of DA spiked into a 5% FBS solution, into a dispersion of D-SWCNTs, and recorded the resulting fluorescence. Similar to the response observed in aqueous solutions to DA (as depicted in **Figure 3 a**), the fluorescence of D-SWCNT E_{11} and E_{11}^* transitions at 992 nm and 1121 nm, respectively, exhibited a concentration-dependent increase upon the addition of DA in a serum environment (**Figure 5 a**). The fluorescence response of both E_{11} and E_{11}^* peaks, which demonstrated enhancement with increasing concentrations of DA, was normalized and fitted using a Hill equation (**Figure 5 b**). The dissociation constant K_d values obtained from the fitting of E_{11} and E_{11}^* were determined to be $84 \pm 30.0\ \mu M$ and $77.6 \pm 26.6\ \mu M$, respectively. Additionally, the LOD for DA by D-SWCNTs was calculated to be 372 ± 156 nM (**Table S3**).

Similarly, different concentrations of serotonin spiked into a 5% FBS solution were introduced with D-SWCNT suspension, and the resulting fluorescence was recorded. A consistent decrease in the fluorescence of D-SWCNTs was observed with the increasing concentration of serotonin, akin to the behavior observed in aqueous solutions of serotonin (**Figure 5 c**). The fluorescence response of both the E_{11} and E_{11}^* peaks, which exhibited a decrease with increasing concentrations of serotonin, was normalized and fitted using a four-parameter logistic function with a zero baseline (**Figure 5 d**). The concentrations of serotonin required for half-maximal response, as determined from fitting E_{11} and E_{11}^*, were found to be 0.8 ± 0.55 μM and 1.8 ± 0.52 μM, respectively. The limit of detection (LOD) was calculated to be 113 ± 27 nM (**Table S4**). Notably, the k_d and LOD values obtained in blood serum and aqueous medium are comparable, indicating the robustness of D-SWCNTs in eliciting divergent responses towards DA and serotonin in different interaction media.

Conversely, pristine SC-SWCNTs, lacking defects, did not exhibit significant changes in fluorescence when exposed to DA or serotonin spiked into 5% FBS (**Figure S 13**). This underscores the crucial role of defects in distinguishing between DA and serotonin, even within a complex biological environment.
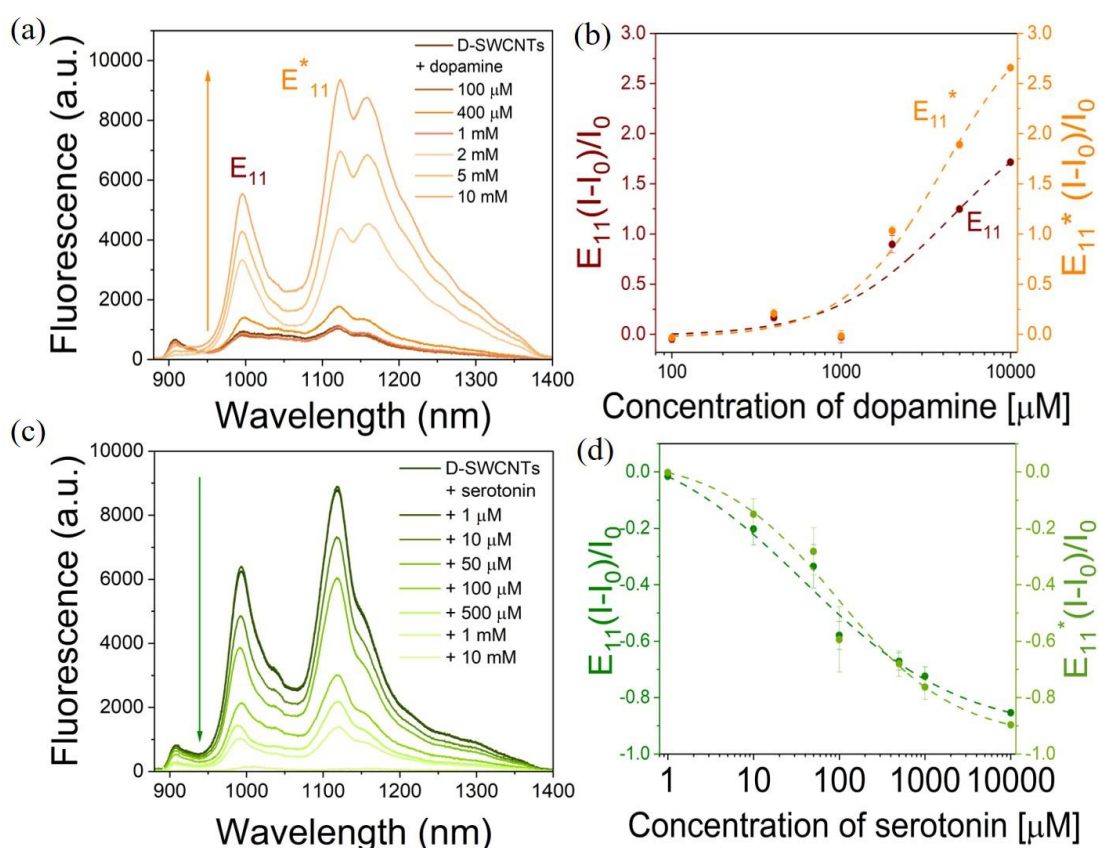
Figure 5 (a) Fluorescence spectra of D-SWCNTs before and after the addition of varying concentrations of DA in FBS. **(b)** Normalized fluorescence response of E_{11} (orange) and E_{11}^* (brown) peaks of D-SWCNTs towards varying concentrations of DA in FBS. **(c)** Fluorescence spectra of D-SWCNTs before and after the addition of varying concentrations of serotonin in FBS. **(d)** Normalized fluorescence response of E_{11} (dark

green) and E_{11}^* (light green) peaks of D-SWCNTs towards varying concentrations of serotonin in FBS.

2.8. Divergent optical responses following the introduction of sp³ defects in SWCNTs stabilized with lipid-PEG corona:

Achieving divergent fluorescence responses to DA and serotonin from D-SWCNTs has so far been explored using SWCNTs stabilized with sodium cholate (SC). In order to lay the groundwork for future advancement and *in vivo* applications, and to further enhance the applicability of the concept developed here, demonstrating the possibility of achieving divergent responses from compositionally similar neurotransmitters using a biocompatible corona could be a significant step forward.

While SC can potentially cause adverse effects in *in vivo* systems, for *in vitro* analyses, such as in complex biological fluids, no such adversity is expected.[73, 74] Nevertheless, to expand the applicability of our approach of using covalent defects to achieve divergent responses of SWCNTs to compositionally similar analytes that would otherwise evoke similar responses, we introduced sp³ defects in SWCNTs suspended with lipid-PEG, namely, 1,2-distearoyl-sn-glycero-3-phosphoethanolamine-N-[carboxy(polyethyleneglycol)-2000] DSPE-PEG. Lipid-PEG is well-recognized for its biocompatibility, and SWCNTs suspended with lipid-PEG have been extensively utilized in biological applications, demonstrating excellent biocompatibility.[74, 75] Our aim was to determine whether, akin to SC-SWCNTs, defects introduced in DSPE-PEG SWCNTs would also enable divergent responses to DA and serotonin.

Specifically, (6,5) chirality-enriched SWCNTs were initially suspended with 2% SC. Subsequently, the SC molecules were replaced with DSPE-PEG via dialysis using standard protocols.[76] The successful replacement of SC with DSPE-PEG was evinced from the bathochromic shift in the absorption peak of the E_{11} transition at 987 nm (**Figure S14 a**).[76] The DSPE-PEG-suspended SWCNTs were then introduced to oxygen defects in a manner similar to that of SC-SWCNTs. Notably, the introduction of oxygen defects resulted in the appearance of the E_{11}^* peak at 1120 nm, akin to what was observed in SC-SWCNTs with defects. The concentration of defects in DSPE-PEG-SWCNTs was adjusted such that the intensity of the peak corresponding to E_{11}^* was approximately half that of E_{11}. Under these conditions, DSPE-PEG-SWCNTs with induced defects (DSPE-PEG-D-SWCNTs) exhibited a significant increase in fluorescence when treated with dopamine (**Figure S 14 b**). Conversely, when treated with serotonin, DSPE-PEG-D-SWCNTs showed a notable decrease in fluorescence (**Figure S14 b**). Importantly, pristine DSPE-PEG-SWCNTs, lacking defects, showed little distinction between dopamine and serotonin, as both resulted in decreased fluorescence of the SWCNTs—albeit to varying degrees (**Figure S 14 c**). These results are similar to those obtained using defects-induced SC-SWCNTs.

These results highlighted that the distinct optical responses of D-SWCNTs to DA and serotonin could be achieved with different corona phases involved in dispersing the D-SWCNTs, thereby underscoring the generality of the approach of introducing oxygen defects to evoke divergent responses from compositionally analogous neurotransmitters, which otherwise produce similar responses from defect-free SWCNTs. Further, this study also lays the foundation for future applications of this

concept in the facile discrimination of neurotransmitters *in vivo*. Another important future research direction could involve monitoring the reversibility of the interaction between compositionally allied neurotransmitters and D-SWCNTs, as well as fluorescence lifetime measurements, to extend our understanding of the photophysical properties of the D-SWCNT interaction with target analytes.

3. Conclusion:

Tuning the optical response of NIR fluorescent SWCNTs toward compositionally similar molecules through incorporating oxygen defects, especially to achieve divergent responses from these similar molecules, remains a persistent challenge. In this study, oxygen defects were introduced in (6,5) enriched SWCNTs by a one-step reaction with NaClO under UV exposure. The successful incorporation of oxygen defects was validated through various analytical techniques, including UV-vis-NIR absorbance, NIR fluorescence, and Raman spectroscopy. Despite sharing similar functional groups, such as aromatic rings, -OH groups, and amine groups, DA and serotonin exhibited notably distinct effects on the fluorescence of D-SWCNTs, while pristine SWCNTs featured rather similar responses to DA and serotonin. Specifically, DA induced a substantial six-fold increase in the fluorescence intensity of D-SWCNTs, while serotonin significantly quenched the fluorescence of D-SWCNTs. Mechanistic investigations elucidated that the enhanced fluorescence of D-SWCNTs upon adding DA could be ascribed to surface adsorption by PDA formed through the polymerization of DA. Conversely, the decreased fluorescence of D-SWCNTs upon adding serotonin was linked to enhanced water accessibility resulting from changes in the surface coverage of SC-SWCNTs. Finally, DA and serotonin were observed to induce distinct responses in the fluorescence of D-SWCNTs even in a serum environment. To the best of our knowledge, this is the first-ever report of using covalent defects in SWCNTs to achieve divergent responses from compositionally analogous neurotransmitters which otherwise featured similar responses in the absence of the defects.

This study is anticipated to deepen our understanding of how defects alter the surface chemistry of SWCNTs, leading to divergent optical responses from molecules that otherwise exhibit similar optical behavior with defect-free SWCNTs. Additionally, this research lays the groundwork for the discrimination of compositionally allied neurotransmitters, addressing a major challenge in the field of neurochemistry.

4. Experimental section:

Dispersion of SWCNTs with sodium cholate: To disperse (6,5) enriched CoMoCaT SWCNTs using sodium cholate (SC), 10 mg of SWCNTs were added to 20 mL of 2% SC. The mixture underwent 10 minutes of bath sonication followed by 30 minutes of tip sonication (12W) for two cycles, resulting in a SWCNT dispersion. Subsequently, the dispersion was ultracentrifuged at 41,300 rpm for 4 hours, discarding the pellet of aggregated SWCNTs, and using the supernatant for further experiments. The concentration of the SC-SWCNTs was determined to be 163.8 mg L^{-1} through UV-vis-NIR absorption spectroscopy with an extinction coefficient of $0.036 \, \text{L} \cdot \text{mg}^{-1} \cdot \text{cm}^{-1}$ at 632 nm.

Absorption: Absorption spectra were obtained using a UV-vis-NIR spectrophotometer (Shimadzu UV-3600 Plus) covering the wavelength range of 300 to 1400 nm.

Introduction of sp^3 oxygen defects in SC-SWCNTs: To induce sp^3 defects in SC-SWCNTs, NaClO was utilized under UV irradiation. In brief, 10 µL of 11% NaClO was mixed with 990 µL of water, resulting in a 0.11% strength aqueous solution of NaClO. Subsequently, 500 µL of this solution was added to 500 µL of water, resulting in a 0.055% strength aqueous solution of NaClO. In a separate microcentrifuge tube, 20 µL of SC-SWCNTs (163.8 mg L^{-1}) was diluted with 480 µL of water. The dispersion of SC-SWCNTs was then added to 500 µL of the 0.055% NaClO solution alongside 100 µL of 0.11% NaClO solution. This dispersion was exposed to UV light at 254 nm. Time-dependent fluorescence spectra of the resulting dispersions were obtained to confirm the incorporation of oxygen defects, as indicated by the emergence of a new peak at 1120 nm. D-SWCNTs$_{E11<E11*}$, D-SWCNTs$_{E11=E11*}$, and D-SWCNTs$_{E11>E11*}$, shown in Figure 3 in the main text, were obtained following exposure of SC-SWCNTs added with said amount of NaClO to UV light for 4 min, 3 min, and 2 min, respectively.

Mass spectrometry: Mass spectra were obtained using an LCMS Xevo–TQD instrument, and subsequent analysis utilized the Agilent 1260 system. The system incorporated a single quadrupole Mass Spectrometric Detector (MSD) equipped with a multimode ionization chamber capable of both Electrospray Ionization (ESI) and Atmospheric Pressure Chemical Ionization (APCI). Mass spectra were acquired in ESI-positive mode.

Fluorescence: Fluorescence emission spectra were recorded from samples in a 96-well plate positioned on the stage of an inverted microscope (Olympus IX73). A 730 nm continuous-wave laser (MDL-MD-730-1.5W, Changchun New Industries) served as the excitation source. The fluorescence emission spectra were resolved by a spectrograph (Spectra Pro HRS-300, Princeton Instruments) with a 500 µm slit-width and a grating density of 150 g mm^{-1}. Recording of the fluorescence intensity spectrum was carried out using a 1D InGaAs array detector (PylonIR, Teledyne Princeton Instruments) with a 3 s exposure time. Excitation-emission maps were generated by sweeping the excitation wavelength range from 450 to 800 nm in 2 nm increments, facilitated by a supercontinuum white-light laser (NKT-photonics, Super-K Extreme).

Raman spectroscopy: Raman spectroscopic measurements were conducted using a confocal micro-Raman (PL) spectrometer (LabRam HR Evolution). The samples were drop-cast onto a glass slide and excited with a 532 nm laser, while measurements were performed using a ×100 objective with a laser power of 100 mW. Spectra were collected in triplicate and are presented as the average of the three measurements.

Fluorometric responses of D-SWCNTs to neurotransmitters and control analytes: In a 96-well plate, 150 µL of as-prepared D-SWCNTs was added with 3 µL of a 10 mM (unless mentioned otherwise) aqueous solution of neurotransmitters and other analytes. The resulting dispersions were subjected to fluorescence spectrum measurement, with all spectra background-subtracted against blank water. Intensity values were obtained at the peak maximum for each spectrum, and the fluorescence responses were normalized to the initial fluorescence intensity, mitigating the influence of absolute

fluorescence counts on quantitative results. The laser power utilized in the experiments ranged from 12 mW to 22 mW.

Divergent responses from DA and serotonin in serum: DA and serotonin were dissolved in 1:20 diluted fetal bovine serum (FBS, Sigma) to attain a concentration of 10 mM of each. Subsequently, the DA and serotonin stock solutions were serially diluted with 1:20 FBS to achieve the desired concentrations for calibrating D-SWCNTs with respect to varying levels of DA and serotonin. For testing, 150 µL of D-SWCNTs was mixed with 3 µL of DA and serotonin at the desired concentrations (diluted in FBS), and the resulting changes in the fluorescence of the D-SWCNTs were recorded.

Suspension of SWCNTs with DSPE-PEG: SC-SWCNTs were exchanged with 1,2-distearoyl-sn-glycero-3-phosphoethanolamine-N-[carboxy(polyethyleneglycol)-2000] (DSPE-PEG) using a dialysis method. Initially, a 5 mg L^{-1} aqueous solution of DSPE-PEG was thoroughly sonicated to ensure full dissolution. Next, 40 mg L^{-1} of SC-SWCNTs was added to this solution to achieve a final concentration of 2 mg L^{-1} for DSPE-PEG. The resulting mixture underwent dialysis against water, over a period of 6 days with daily water changes. This purpose was to completely remove SC from the SWCNT surface, facilitating the adsorption of DSPE-PEG onto the SWCNTs.

Statistical Analysis: Each sample's fluorescence spectra were normalized to their initial fluorescence intensity. All fluorescence experiments were performed in triplicate, and the presented spectra are the mean of three independently acquired spectra. The fluorescence responses, illustrated in bar diagrams, represent averages of three independent measurements, with accompanying error bars denoting the standard deviation. Spectral data were plotted and analyzed using Origin software, while the excitation and emission profiles were graphed using MATLAB.

Acknowledgments

References:

1.   Chen, J.; Fasihianifard, P.; Raz, A. A. P.; Hickey, B. L.; Moreno, J. L.; Chang, C.-E. A.; Hooley, R. J.; Zhong, W., Selective recognition and discrimination of single isomeric changes in peptide strands with a host : guest sensing array. *Chemical Science* **2024,** *15* (5), 1885-1893.

2.   Yang, H.; Lu, F.; Sun, Y.; Yuan, Z.; Lu, C., Fluorescent Gold Nanocluster-Based Sensor Array for Nitrophenol Isomer Discrimination via an Integration of Host–Guest Interaction and Inner Filter Effect. *Analytical Chemistry* **2018,** *90* (21), 12846-12853.

3.   Ma, C.; Mohr, J. M.; Lauer, G.; Metternich, J. T.; Neutsch, K.; Ziebarth, T.; Reiner, A.; Kruss, S., Ratiometric Imaging of Catecholamine Neurotransmitters with Nanosensors. *Nano Letters* **2024,** *24* (7), 2400-2407.

4.	Beyene, A. G.; Alizadehmojarad, A. A.; Dorlhiac, G.; Goh, N.; Streets, A. M.; Král, P.; Vuković, L.; Landry, M. P., Ultralarge Modulation of Fluorescence by Neuromodulators in Carbon Nanotubes Functionalized with Self-Assembled Oligonucleotide Rings. *Nano Letters* **2018,** *18* (11), 6995-7003.

5.	Krasley, A. T.; Li, E.; Galeana, J. M.; Bulumulla, C.; Beyene, A. G.; Demirer, G. S., Carbon Nanomaterial Fluorescent Probes and Their Biological Applications. *Chemical Reviews* **2024**.

6.	Wang, H.; Boghossian, A. A., Covalent conjugation of proteins onto fluorescent single-walled carbon nanotubes for biological and medical applications. *Mater. Adv.* **2023,** *4* (3), 823-834.

7.	Yoon, M.; Lee, Y.; Lee, S.; Cho, Y.; Koh, D.; Shin, S.; Tian, C.; Song, Y.; Kang, J.; Cho, S.-Y., A nIR fluorescent single walled carbon nanotube sensor for broad-spectrum diagnostics. *Sensors & Diagnostics* **2024**.

8.	Ackermann, J.; Metternich, J. T.; Herbertz, S.; Kruss, S., Biosensing with Fluorescent Carbon Nanotubes. Angew. Chem. **2022,** *61* (18), e202112372.

9.	Farrera, C.; Torres Andón, F.; Feliu, N., Carbon Nanotubes as Optical Sensors in Biomedicine. *ACS Nano* **2017,** *11* (11), 10637-10643.

10.	Satishkumar, B. C.; Brown, L. O.; Gao, Y.; Wang, C.-C.; Wang, H.-L.; Doorn, S. K., Reversible fluorescence quenching in carbon nanotubes for biomolecular sensing. *Nature Nanotechnology* **2007,** *2* (9), 560-564.

11.	Nelson, J. T.; Kim, S.; Reuel, N. F.; Salem, D. P.; Bisker, G.; Landry, M. P.; Kruss, S.; Barone, P. W.; Kwak, S.; Strano, M. S., Mechanism of Immobilized Protein A Binding to Immunoglobulin G on Nanosensor Array Surfaces. *Analytical Chemistry* **2015,** *87* (16), 8186-8193.

12.	Williams, R. M.; Lee, C.; Heller, D. A., A Fluorescent Carbon Nanotube Sensor Detects the Metastatic Prostate Cancer Biomarker uPA. *ACS Sensors* **2018,** *3* (9), 1838-1845.

13.	Antman-Passig, M.; Yaari, Z.; Goerzen, D.; Parikh, R.; Chatman, S.; Komer, L. E.; Chen, C.; Grabarnik, E.; Mathieu, M.; Haimovitz-Friedman, A.; Heller, D. A., Nanoreporter Identifies Lysosomal Storage Disease Lipid Accumulation Intracranially. *Nano Letters* **2023,** *23* (23), 10687-10695.

14.	Zubkovs, V.; Schuergers, N.; Lambert, B.; Ahunbay, E.; Boghossian, A. A., Mediatorless, Reversible Optical Nanosensor Enabled through Enzymatic Pocket Doping. Small **2017,** *13* (42), 1701654.

15.	Karachevtsev, V. A.; Glamazda, A. Y.; Leontiev, V. S.; Lytvyn, O. S.; Dettlaff-Weglikowska, U., Glucose sensing based on NIR fluorescence of DNA-wrapped single-walled carbon nanotubes. *Chem. Phys. Lett.* **2007,** *435* (1), 104-108.

16.	Nishitani, S.; Tran, T.; Puglise, A.; Yang, S.; Landry, M. P., Engineered Glucose Oxidase-Carbon Nanotube Conjugates for Tissue-Translatable Glucose Nanosensors. Angew. Chem. 2024, e202311476.

17.	Wulf, V.; Bichachi, E.; Hendler-Neumark, A.; Massarano, T.; Leshem, A. B.; Lampel, A.; Bisker, G., Multicomponent System of Single-Walled Carbon Nanotubes Functionalized with a Melanin-Inspired Material for Optical Detection and Scavenging of Metals. Adv Func Mater **2022,** *32* (49), 2209688.

18.	Amir, D.; Hendler-Neumark, A.; Wulf, V.; Ehrlich, R.; Bisker, G., Oncometabolite Fingerprinting Using Fluorescent Single-Walled Carbon Nanotubes. Adv Mater Interfaces **2022,** *9* (4), 2101591.

19.	Shumeiko, V.; Paltiel, Y.; Bisker, G.; Hayouka, Z.; Shoseyov, O., A nanoscale paper-based near-infrared optical nose (NIRON). *Biosensors and Bioelectronics* **2021,** *172*, 112763.

20.	Shumeiko, V.; Malach, E.; Helman, Y.; Paltiel, Y.; Bisker, G.; Hayouka, Z.; Shoseyov, O., A nanoscale optical biosensor based on peptide encapsulated SWCNTs for detection of acetic acid in the gaseous phase. *Sensors and Actuators B: Chemical* **2021,** *327*, 128832.

21.   Nißler, R.; Bader, O.; Dohmen, M.; Walter, S. G.; Noll, C.; Selvaggio, G.; Groß, U.; Kruss, S., Remote near infrared identification of pathogens with multiplexed nanosensors. *Nat Commun* **2020,** *11* (1), 5995.

22.   Shumeiko, V.; Zaken, Y.; Hidas, G.; Paltiel, Y.; Bisker, G.; Shoseyov, O., Peptide-Encapsulated Single-Wall Carbon Nanotube-Based Near-Infrared Optical Nose for Bacteria Detection and Classification. *IEEE Sensors Journal* **2022,** *22* (7), 6277-6287.

23.   Hendler-Neumark, A.; Wulf, V.; Bisker, G., Single-Walled Carbon Nanotube Sensor Selection for the Detection of MicroRNA Biomarkers for Acute Myocardial Infarction as a Case Study. *ACS Sensors* **2023**.

24.   Harvey, J. D.; Jena, P. V.; Baker, H. A.; Zerze, G. H.; Williams, R. M.; Galassi, T. V.; Roxbury, D.; Mittal, J.; Heller, D. A., A carbon nanotube reporter of microRNA hybridization events in vivo. *Nature Biomedical Engineering* **2017,** *1* (4), 0041.

25.   Mann, F. A.; Herrmann, N.; Meyer, D.; Kruss, S., Tuning Selectivity of Fluorescent Carbon Nanotube-Based Neurotransmitter Sensors. *Sensors* **2017,** *17* (7), 1521.

26.   Ackermann, J.; Stegemann, J.; Smola, T.; Reger, E.; Jung, S.; Schmitz, A.; Herbertz, S.; Erpenbeck, L.; Seidl, K.; Kruss, S., High Sensitivity Near-Infrared Imaging of Fluorescent Nanosensors. Small **2023,** *19* (14), 2206856.

27.   Nißler, R.; Mann, F. A.; Preiß, H.; Selvaggio, G.; Herrmann, N.; Kruss, S., Chirality enriched carbon nanotubes with tunable wrapping via corona phase exchange purification (CPEP). *Nanoscale* **2019,** *11* (23), 11159-11166.

28.   Chio, L.; Pinals, R. L.; Murali, A.; Goh, N. S.; Landry, M. P., Covalent Surface Modification Effects on Single-Walled Carbon Nanotubes for Targeted Sensing and Optical Imaging. Adv Func Mater **2020,** *30* (17), 1910556.

29.   Jeong, S.; Yang, D.; Beyene, A. G.; Del Bonis-O'Donnell, J. T.; Gest, A. M. M.; Navarro, N.; Sun, X.; Landry, M. P., High-throughput evolution of near-infrared serotonin nanosensors. *Sci Adv.* **2019,** *5* (12), eaay3771.

30.   Basu, S.; Hendler-Neumark, A.; Bisker, G., Rationally Designed Functionalization of Single-Walled Carbon Nanotubes for Real-Time Monitoring of Cholinesterase Activity and Inhibition in Plasma. *Small* 2024, 2309481.

31.   Basu, S.; Hendler-Neumark, A.; Bisker, G., Monitoring Enzyme Activity Using Near-Infrared Fluorescent Single-Walled Carbon Nanotubes. *ACS Sensors* **2024,** *9* (5), 2237-2253.

32.   Kuo, M.-T.; Raffaelle, J. F.; Waller, E. M.; Varaljay, V. A.; Wagner, D.; Kelley-Loughnane, N.; Reuel, N. F., Screening Enzymatic Degradation of Polyester Polyurethane with Fluorescent Single-walled Carbon Nanotube and Polymer Nanoparticle Conjugates. *ACS Nano* **2023**.

33.   Ma, C.; Schrage, C. A.; Gretz, J.; Akhtar, A.; Sistemich, L.; Schnitzler, L.; Li, H.; Tschulik, K.; Flavel, B. S.; Kruss, S., Stochastic Formation of Quantum Defects in Carbon Nanotubes. *ACS Nano* **2023,** *17* (16), 15989-15998.

34.   Ghosh, S.; Bachilo, S. M.; Simonette, R. A.; Beckingham, K. M.; Weisman, R. B., Oxygen Doping Modifies Near-Infrared Band Gaps in Fluorescent Single-Walled Carbon Nanotubes. *Science* **2010,** *330* (6011), 1656-1659.

35.   Mandal, A. K.; Wu, X.; Ferreira, J. S.; Kim, M.; Powell, L. R.; Kwon, H.; Groc, L.; Wang, Y.; Cognet, L., Fluorescent sp3 Defect-Tailored Carbon Nanotubes Enable NIR-II Single Particle Imaging in Live Brain Slices at Ultra-Low Excitation Doses. *Sci rep* **2020,** *10* (1), 5286.

36.   Zou, Y.; Nishina, Y.; Bianco, A., The use of covalent reactions to improve the biomedical applications of carbon nanomaterials. *Carbon Reports* **2023,** *2* (4), 185-198.

37.   Janas, D., Perfectly imperfect: a review of chemical tools for exciton engineering in single-walled carbon nanotubes. *Mater. Horiz.* **2020,** *7* (11), 2860-2881.

38.   Nakajima, H.; Kobashi, K.; Zhou, Y.; Zhang, M.; Okazaki, T., Quantitative analysis of the correlation between sp3 bonds and functional groups in covalently functionalized single-walled carbon nanotubes. *Carbon* **2024,** *216*, 118495.

39.   Setaro, A.; Adeli, M.; Glaeske, M.; Przyrembel, D.; Bisswanger, T.; Gordeev, G.; Maschietto, F.; Faghani, A.; Paulus, B.; Weinelt, M.; Arenal, R.; Haag, R.; Reich, S., Preserving π-conjugation in covalently functionalized carbon nanotubes for optoelectronic applications. *Nat Commun* **2017,** *8* (1), 14281.

40.   Trerayapiwat, K. J.; Li, X.; Ma, X.; Sharifzadeh, S., Broken Symmetry Optical Transitions in (6,5) Single-Walled Carbon Nanotubes Containing sp3 Defects Revealed by First-Principles Theory. *Nano Letters* **2024,** *24* (2), 667-671.

41.   Niidome, Y.; Wakabayashi, R.; Goto, M.; Fujigaya, T.; Shiraki, T., Protein-structure-dependent spectral shifts of near-infrared photoluminescence from locally functionalized single-walled carbon nanotubes based on avidin–biotin interactions. *Nanoscale* **2022,** *14* (36), 13090-13097.

42.   Piao, Y.; Meany, B.; Powell, L. R.; Valley, N.; Kwon, H.; Schatz, G. C.; Wang, Y., Brightening of carbon nanotube photoluminescence through the incorporation of sp3 defects. *Nature Chemistry* **2013,** *5* (10), 840-845.

43.   Kim, M.; McCann, J. J.; Fortner, J.; Randall, E.; Chen, C.; Chen, Y.; Yaari, Z.; Wang, Y.; Koder, R. L.; Heller, D. A., Quantum Defect Sensitization via Phase-Changing Supercharged Antibody Fragments. *J. Am. Chem. Soc.* **2024,** *146* (18), 12454-12462.

44.   Zheng, Y.; Alizadehmojarad, A. A.; Bachilo, S. M.; Weisman, R. B., Guanine-Specific Chemical Reaction Reveals ssDNA Interactions on Carbon Nanotube Surfaces. *J. Phys. Chem. Lett.* **2022,** *13* (9), 2231-2236.

45.   Spreinat, A.; Dohmen, M. M.; Lüttgens, J.; Herrmann, N.; Klepzig, L. F.; Nißler, R.; Weber, S.; Mann, F. A.; Lauth, J.; Kruss, S., Quantum Defects in Fluorescent Carbon Nanotubes for Sensing and Mechanistic Studies. *J. Phys. Chem. C* **2021,** *125* (33), 18341-18351.

46.   Galonska, P.; Mohr, J. M.; Schrage, C. A.; Schnitzler, L.; Kruss, S., Guanine Quantum Defects in Carbon Nanotubes for Biosensing. *J. Phys. Chem. Lett.* **2023,** *14* (14), 3483-3490.

47.   Sebastian, F. L.; Becker, F.; Yomogida, Y.; Hosokawa, Y.; Settele, S.; Lindenthal, S.; Yanagi, K.; Zaumseil, J., Unified Quantification of Quantum Defects in Small-Diameter Single-Walled Carbon Nanotubes by Raman Spectroscopy. *ACS Nano* **2023,** *17* (21), 21771-21781.

48.   Kim, M.; Chen, C.; Yaari, Z.; Frederiksen, R.; Randall, E.; Wollowitz, J.; Cupo, C.; Wu, X.; Shah, J.; Worroll, D.; Lagenbacher, R. E.; Goerzen, D.; Li, Y.-M.; An, H.; Wang, Y.; Heller, D. A., Nanosensor-based monitoring of autophagy-associated lysosomal acidification in vivo. *Nature Chemical Biology* **2023**.

49.   Da, Y.; Luo, S.; Tian, Y., Real-Time Monitoring of Neurotransmitters in the Brain of Living Animals. *ACS Appl. Mater. Interfaces* **2023,** *15* (1), 138-157.

50.   Nakatsuka, N.; Andrews, A. M., Differentiating Siblings: The Case of Dopamine and Norepinephrine. *ACS Chemical Neuroscience* **2017,** *8* (2), 218-220.

51.   Lin, C.-W.; Bachilo, S. M.; Zheng, Y.; Tsedev, U.; Huang, S.; Weisman, R. B.; Belcher, A. M., Creating fluorescent quantum defects in carbon nanotubes using hypochlorite and light. *Nat Commun* **2019,** *10* (1), 2874.

52.   Ma, X.; Adamska, L.; Yamaguchi, H.; Yalcin, S. E.; Tretiak, S.; Doorn, S. K.; Htoon, H., Electronic Structure and Chemical Nature of Oxygen Dopant States in Carbon Nanotubes. *ACS Nano* **2014,** *8* (10), 10782-10789.

53.   Gifford, B. J.; Kilina, S.; Htoon, H.; Doorn, S. K.; Tretiak, S., Controlling Defect-State Photophysics in Covalently Functionalized Single-Walled Carbon Nanotubes. *Accounts of Chemical Research* **2020,** *53* (9), 1791-1801.

54.   Sebastian, F. L.; Zorn, N. F.; Settele, S.; Lindenthal, S.; Berger, F. J.; Bendel, C.; Li, H.; Flavel, B. S.; Zaumseil, J., Absolute Quantification of sp3 Defects in Semiconducting Single-Wall Carbon Nanotubes by Raman Spectroscopy. *J. Phys. Chem. Lett.* **2022,** *13* (16), 3542-3548.

55.   Saha, A.; Gifford, B. J.; He, X.; Ao, G.; Zheng, M.; Kataura, H.; Htoon, H.; Kilina, S.; Tretiak, S.; Doorn, S. K., Narrow-band single-photon emission through selective aryl functionalization of zigzag carbon nanotubes. *Nature Chemistry* **2018,** *10* (11), 1089-1095.

56.   He, X.; Gifford, B. J.; Hartmann, N. F.; Ihly, R.; Ma, X.; Kilina, S. V.; Luo, Y.; Shayan, K.; Strauf, S.; Blackburn, J. L.; Tretiak, S.; Doorn, S. K.; Htoon, H., Low-Temperature Single Carbon Nanotube Spectroscopy of sp3 Quantum Defects. *ACS Nano* **2017,** *11* (11), 10785-10796.

57.   Zheng, Y.; Han, Y.; Weight, B. M.; Lin, Z.; Gifford, B. J.; Zheng, M.; Kilin, D.; Kilina, S.; Doorn, S. K.; Htoon, H.; Tretiak, S., Photochemical spin-state control of binding configuration for tailoring organic color center emission in carbon nanotubes. *Nat Commun* **2022,** *13* (1), 4439.

58.   Tanwar, A. S.; Parui, R.; Garai, R.; Chanu, M. A.; Iyer, P. K., Dual "Static and Dynamic" Fluorescence Quenching Mechanisms Based Detection of TNT via a Cationic Conjugated Polymer. *ACS Measurement Science Au* **2022,** *2* (1), 23-30.

59.   Dizman, H. M.; Arsu, N., Rapid and sensitive colorimetric determination of dopamine and serotonin in solution and polymer matrix with photochemically prepared and N-acetyl-L-cysteine functionalized gold nanoparticles. *Materials Today Communications* **2023,** *35*, 105599.

60.   Wetzl, C.; Brosel-Oliu, S.; Carini, M.; Di Silvio, D.; Illa, X.; Villa, R.; Guimera, A.; Prats-Alfonso, E.; Prato, M.; Criado, A., Covalent functionalisation controlled by molecular design for the aptameric recognition of serotonin in graphene-based field-effect transistors. *Nanoscale* **2023,** *15* (41), 16650-16657.

61.   Anastassiou, C. A.; Patel, B. A.; Arundell, M.; Yeoman, M. S.; Parker, K. H.; O'Hare, D., Subsecond Voltammetric Separation between Dopamine and Serotonin in the Presence of Ascorbate. *Analytical Chemistry* **2006,** *78* (19), 6990-6998.

62.   Tiwari, A.; Walia, S.; Sharma, S.; Chauhan, S.; Kumar, M.; Gadly, T.; Randhawa, J. K., High quantum yield carbon dots and nitrogen-doped carbon dots as fluorescent probes for spectroscopic dopamine detection in human serum. *J Mater Chem B* **2023,** *11* (5), 1029-1043.

63.   Kruss, S.; Landry, M. P.; Vander Ende, E.; Lima, B. M. A.; Reuel, N. F.; Zhang, J.; Nelson, J.; Mu, B.; Hilmer, A.; Strano, M., Neurotransmitter Detection Using Corona Phase Molecular Recognition on Fluorescent Single-Walled Carbon Nanotube Sensors. *J. Am. Chem. Soc.* **2014,** *136* (2), 713-724.

64.   Bregnhøj, M.; Westberg, M.; Jensen, F.; Ogilby, P. R., Solvent-dependent singlet oxygen lifetimes: temperature effects implicate tunneling and charge-transfer interactions. *Phys Chem Chem Phys* **2016,** *18* (33), 22946-22961.

65.   Dutt, V. G. V.; Akhil, S.; Mishra, N., Surface Passivation Strategies for Improving Photoluminescence and Stability of Cesium Lead Halide Perovskite Nanocrystals. ChemNanoMat **2020,** *6* (12), 1730-1742.

66.   Li, X.; Zhang, S.; Kulinich, S. A.; Liu, Y.; Zeng, H., Engineering surface states of carbon dots to achieve controllable luminescence for solid-luminescent composites and sensitive Be2+ detection. *Sci rep* **2014,** *4* (1), 4976.

67.   Dong, W.; Qiao, W.; Xiong, S.; Yang, J.; Wang, X.; Ding, L.; Yao, Y.; Bao, Q., Surface Passivation and Energetic Modification Suppress Nonradiative Recombination in Perovskite Solar Cells. *Nano-Micro Letters* **2022,** *14* (1), 108.

68.   Xu, L.; Li, J.; Cai, B.; Song, J.; Zhang, F.; Fang, T.; Zeng, H., A bilateral interfacial passivation strategy promoting efficiency and stability of perovskite quantum dot light-emitting diodes. *Nat Commun* **2020,** *11* (1), 3902.

69.   Chen, S. L.; Chen, W. M.; Ishikawa, F.; Buyanova, I. A., Suppression of non-radiative surface recombination by N incorporation in GaAs/GaNAs core/shell nanowires. *Sci rep* **2015,** *5* (1), 11653.

70.   Pappalardo, J. S.; Macairan, J.-R.; Macina, A.; Poulhazan, A.; Quattrocchi, V.; Marcotte, I.; Naccache, R., Effects of polydopamine-passivation on the optical properties of carbon dots and its potential use in vivo. *Phys Chem Chem Phys* **2020,** *22* (29), 16595-16605.

71.   Lyu, Q.; Hsueh, N.; Chai, C. L. L., Unravelling the polydopamine mystery: is the end in sight? *Polymer Chemistry* **2019,** *10* (42), 5771-5777.

72.   Paillard, V., On the origin of the 1100 cm−1 Raman band in amorphous and nanocrystalline sp3 carbon. *Europhysics Letters* **2001,** *54* (2), 194.

73.   Gillen, A. J.; Siefman, D. J.; Wu, S.-J.; Bourmaud, C.; Lambert, B.; Boghossian, A. A., Templating colloidal sieves for tuning nanotube surface interactions and optical sensor responses. *Journal of Colloid and Interface Science* **2020,** *565*, 55-62.

74.   Kim, M.; Goerzen, D.; Jena, P. V.; Zeng, E.; Pasquali, M.; Meidl, R. A.; Heller, D. A., Human and environmental safety of carbon nanotubes across their life cycle. *Nature Reviews Materials* **2024,** *9* (1), 63-81.

75.   Levin, N.; Hendler-Neumark, A.; Kamber, D.; Bisker, G., Enhanced cellular internalization of near-infrared fluorescent single-walled carbon nanotubes facilitated by a transfection reagent. *Journal of Colloid and Interface Science* **2024,** *664*, 650-666.

76.   Bisker, G.; Dong, J.; Park, H. D.; Iverson, N. M.; Ahn, J.; Nelson, J. T.; Landry, M. P.; Kruss, S.; Strano, M. S., Protein-targeted corona phase molecular recognition. *Nat Commun* **2016,** *7* (1), 10241.

Table of contents graphics: